

# First results from the new PVLAS apparatus: a new limit on vacuum magnetic birefringence

F. Della Valle and E. Milotti

*INFN, Sezione di Trieste and Dipartimento di Fisica,  
Università di Trieste, Via Valerio 2, I-34127 Trieste, Italy*

A. Ejlli, G. Messineo, L. Piemontese, and G. Zavattini

*INFN, Sezione di Ferrara and Dipartimento di Fisica, Università di Ferrara,  
Polo Scientifico, Via Saragat 1 C, I-44100 Ferrara, Italy*

U. Gastaldi

*INFN, Sezione di Ferrara, Polo Scientifico, Via Saragat 1 C, I-44100 Ferrara, Italy*

R. Pengo and G. Ruoso

*INFN, Laboratori Nazionali di Legnaro, Viale dell'Università 2, I-35020 Legnaro*

(Dated: December 6, 2024)

Several groups are carrying out experiments to observe and measure vacuum magnetic birefringence, predicted by Quantum Electrodynamics (QED). We have started running the new PVLAS apparatus installed in Ferrara and have measured a noise floor value for the unitary field magnetic birefringence of vacuum  $\Delta n_u^{(\text{vac})} = (4 \pm 20) \times 10^{-23} \text{ T}^{-2}$  (the error represents a  $1\sigma$  deviation). From this measurement one can extract a new limit on  $A_e$ , the parameter describing non linear effects in QED:  $A_e < 65 \times 10^{-24} \text{ T}^{-2}$ . This result represents an improvement by a factor 20 in comparison to previous measurements and reduces to a factor 50 the gap to be overcome to measure for the first time the value of  $A_e$  predicted by QED:  $A_e = 1.32 \times 10^{-24} \text{ T}^{-2}$ . These birefringence measurements also yield an almost ten-fold improvement on model-independent bounds on the coupling constant of axion-like particles to two photons, for masses greater than 1 meV, along with a factor two improvement of the limit on millicharged particles (fermions and scalars), including neutrinos.

PACS numbers: 12.20.Fv, 42.50.Xa, 07.60.Fs

## I. INTRODUCTION

Non linear electrodynamic effects in vacuum have been predicted since the earliest days of Quantum Electrodynamics (QED), a few years after the discovery of positrons [1–3]. One such effect is vacuum magnetic birefringence [4], closely connected to light-light interaction. This effect is due to the magnetic polarizability of vacuum associated to the zero-point fluctuations of charged fermion fields. Virtual electron-positron pairs account for most of vacuum magnetic birefringence. The overall effect is extremely small and has never yet been observed directly. The birefringence induced by an external magnetic field  $B$  is given, to the lowest order, by the simple expression [4]

$$\Delta n^{(\text{QED})} = 3A_e B^2 \quad (1)$$

where the parameter  $A_e$  determines the strength of the non-linear terms in the QED Lagrangian [1]:

$$L_{\text{EHW}} = \frac{A_e}{\mu_0} \left[ \left( \frac{E^2}{c^2} - B^2 \right)^2 + 7 \left( \frac{\vec{E}}{c} \cdot \vec{B} \right)^2 \right] \quad (2)$$

where

$$A_e = \frac{2}{45\mu_0} \frac{\alpha^2 \lambda_e^3}{m_e c^2} = 1.32 \times 10^{-24} \text{ T}^{-2}. \quad (3)$$

Here  $\lambda_e$  is the Compton wavelength of the electron,  $\alpha = e^2/(\hbar c 4\pi\epsilon_0)$  the fine structure constant,  $m_e$  the electron mass,  $c$  the speed of light in vacuum, and  $\mu_0$  the magnetic permeability of vacuum.

In analogy to what is done for the Cotton-Mouton effect (for a review see [5]), one can define the unitary field magnetic birefringence of vacuum  $\Delta n_u^{(\text{vac})}$  by dividing the vacuum magnetic birefringence (1) by  $B^2$ . Indeed vacuum magnetic birefringence depends on  $B^2$  as do the Cotton-Mouton effect, axion-like particle (ALP) induced birefringence and millicharged particle induced birefringence. These last two hypothetical effects represent new physics beyond the Standard Model and can be searched for in a model independent way with an apparatus such as PVLAS [6–10].

The ellipticity  $\psi$  induced on a beam of linearly polarized laser light of wavelength  $\lambda$  which traverses a vacuum region of length  $L$ , where a magnetic field  $B$  orthogonal to the direction of light propagation is present, is given by [11–15]

$$\psi = \frac{N\pi\Delta n_u^{(\text{vac})}}{\lambda} \int B^2 dl \sin 2\vartheta \quad (4)$$

where  $\vartheta$  is the angle between the directions of the polarization vector and of the magnetic field vector and  $N$  is the number of times the medium is traversed by the light.

An ellipsometric method to observe vacuum magnetic birefringence was proposed by E. Iacopini and E. Zavattini in 1979 [11]. Experimental attempts started in the nineties [6, 12] and several are ongoing [9, 10, 13–16]. The nonlinear parameter  $A_e$  can also be measured by direct light-light scattering experiments [17–22]. Neither method has reached the capability of detecting this fundamental nonlinear effect in QED vacuum regarding light by light interaction. Presently published limits on  $A_e$  determined from ellipsometric experiments are reported in Table I.

Table I: Presently published upper bounds of  $A_e$  obtained from ellipsometric measurements.

Experiment	Limit ( $10^{-24} \text{ T}^{-2}$ )	Reference
BFRT	135000 @ 95% c.l.	[6]
PVLAS - LNL	6600 @ 95% c.l.	[13]
PVLAS - FE test setup	3300 @ 95% c.l.	[14]
BMV	2700 @ 99.7% c.l.	[23]

In this letter we report on a significant improvement obtained after the commissioning of the new PVLAS experimental setup installed at the INFN section of Ferrara. We have obtained a new upper limit for the parameter  $A_e$ , which improves by a factor of about 20 on the previously published results:

$$A_e < 65 \times 10^{-24} \text{ T}^{-2} @ 68\% \text{ c.l.} \quad (5)$$

The principle of the experiment is explained in [11, 14]. The calibration of the apparatus has been done by measuring the Cotton-Mouton effect of  $\text{O}_2$  and He gases at low pressures and controlling their consistency with the values present in literature. In this paper we briefly summarize the main features of the new experimental setup and focus on the measurements giving a new conservative upper limit on  $A_e$ .

## II. EXPERIMENTAL METHOD AND APPARATUS

The upper and lower panels of figure 1 show a schematic top view and a photograph of the apparatus.

A solid state Nd:YAG NPRO laser ( $\lambda = 1064 \text{ nm}$ ) injects linearly polarized light into the ellipsometer which is installed inside a high vacuum enclosure. The ellipsometer consists of an entrance polarizer **P** and an analyzer **A** set to maximum extinction. Between **P** and **A** are installed the entrance mirror **M1** and the exit mirror **M2** of a Fabry-Perot 3.303 m long cavity **FP** with ultra-high finesse  $\mathcal{F} \approx 670000$  [24]. The light back-reflected by the **FP** is detected by the photodiode **PRF**, and is used by a feedback system which locks the laser frequency to the **FP** with a variant of the Pound-Drever-Hall technique [25]. The resonant light between the two mirrors traverses the bore of two identical permanent dipole magnets (see Table II). The magnets can rotate around the

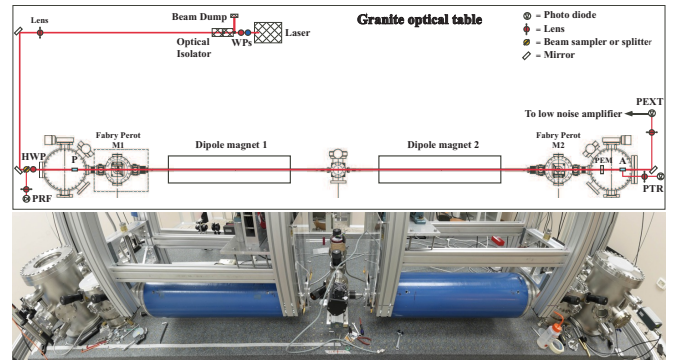


Figure 1: Upper panel: Scheme of the apparatus. The granite optical table, 4.8 m x 1.5 m, is shown together with the optical components and the five vacuum chambers. **HWP** = Half wave plate; **P** = Polarizer; **A** = Analyzer; **WPs** = Wave plates; **PEM** = Photoelastic Modulator; **PRF** = Reflection photodiode; **PTR** = Transmission photodiode; **PEXT** = Extinction photodiode. Lower panel: A wide-angle picture of the PVLAS apparatus. The two blue cylinders are the permanent magnets: they are hanging from an aluminium structure mechanically decoupled from the rest of the optical table.

Table II: Magnet characteristics.

Components	2 permanent dipole magnets in Halbach configuration. Central bore 20 mm Physical length 96 cm External diameter 28 cm Include a magnetic field shielding.
Field strength	$B_{\max} = 2.6 \text{ T}$ $\int B^2 dl = 5.12 \text{ T}^2\text{m}$ each. Stray field < 1 gauss (along axis @ 20 cm).
Rotation frequency	Up to 10 Hz.

**FP** cavity axis so that the magnetic field vectors of the two magnets rotate in planes normal to the path of the light stored in the cavity. The motors driving the two magnets are controlled by two phase locked signal generators. The same signal generators trigger the data acquisition. The magnetic field of the magnets induce a birefringence on the medium in the bores; the **FP** enhances the ellipticity acquired by the light by a factor  $N = 2\mathcal{F}/\pi$ . Due to the rotation of the magnetic field, the induced ellipticity varies harmonically at twice the rotation frequency of the magnets [see the dependence of  $\psi$  from  $2\vartheta$  in equation (4)]. Given the parameters of our apparatus ( $\lambda = 1064 \text{ nm}$ ,  $\int B^2 dl = 10.25 \text{ T}^2\text{m}$ ) the predicted ellipticity generated by vacuum magnetic birefringence after a single passage of the light through the magnets is  $\psi_{\text{single}} = 1.2 \times 10^{-16}$ . The **FP** cavity multiplies the single pass ellipticity  $\psi_{\text{single}}$  by a factor  $N = 4.3 \times 10^5$ , resulting in an ellipticity to be measured of  $\psi^{(\text{QED})} = 5 \times 10^{-11}$ .

A photo elastic modulator (**PEM**) then adds a known

oscillating small ellipticity  $\eta(t)$  of amplitude  $\eta_0 \approx 10^{-3}$  at a fixed frequency  $\Omega_{\text{PEM}} \approx 314$  krad/s. Under these conditions the intensity  $I_{\text{out}}(t)$  of the light emerging from the analyzer **A** is

$$I_{\text{out}}(t) = I_0 \left[ \sigma^2 + |\eta(t) + \psi \sin 2\vartheta(t) + \alpha(t)|^2 \right] \simeq I_0 \left[ \sigma^2 + \eta(t)^2 + 2\eta(t)\psi \sin 2\vartheta(t) + 2\eta(t)\alpha(t) \right] \quad (6)$$

where  $I_0$  represents the light power reaching the analyzer,  $\sigma^2$  (nominally  $\lesssim 10^{-7}$ ) is the extinction ratio of the two polarisers and  $\alpha(t)$  describes the slowly varying spurious ellipticities present in the apparatus. As can be seen, the introduction of the **PEM** linearises the ellipticity signal which would otherwise be quadratic. The light emerging from the analyzer is collected by the photodiode **PEXT**.

The most important Fourier components of  $I_{\text{out}}(t)$  come from the terms  $2\eta(t)\psi \sin 2\vartheta(t)$  and  $\eta(t)^2$ . The first of these terms results in the beating of the ellipticity induced by the **PEM** (at  $\Omega_{\text{PEM}}$ ) and the ellipticity induced by the rotating magnets (at  $2\Omega_{\text{Mag}}$ ). The term  $\eta(t)^2$  generates a Fourier component at  $2\Omega_{\text{PEM}}$ .

During acquisition the photodiode signal coming from **PEXT** is demodulated at the frequency  $\Omega_{\text{PEM}}$  and at its second harmonic  $2\Omega_{\text{PEM}}$ . Both these demodulated signals, respectively  $I_{\Omega_{\text{PEM}}}(t)$  and  $I_{2\Omega_{\text{PEM}}}(t)$ , are acquired by a data acquisition system together with the ordinary beam intensity  $I_0$  exiting the analyzer **A**. With the DC component of  $I_{2\Omega_{\text{PEM}}}(t)$ , indicated as  $I_{2\Omega_{\text{PEM}}}(\text{DC})$ , and  $I_{\Omega_{\text{PEM}}}(t)$  the ellipticity signal  $\psi(t)$  can be determined by the equation

$$\psi(t) = \frac{I_{\Omega_{\text{PEM}}}(t)}{\sqrt{8I_0 I_{2\Omega_{\text{PEM}}}(\text{DC})}}. \quad (7)$$

With the magnets rotating at  $\Omega_{\text{Mag}}$ , a magnetically induced birefringence generates a Fourier component of  $\psi(t)$  at  $2\Omega_{\text{Mag}}$ .

Magnetic field sensors and laser locking signals are also acquired to determine the phase of  $\psi(t)$  and for diagnostics. These signals are sampled at 32 times the rotation frequency of the magnets (typically 3 Hz) by a 16 bit multi channel ADC board.

The vacuum system must guarantee that the presence of residual gas species do not mask vacuum magnetic birefringence. Indeed the Cotton-Mouton effect induces a magnetic birefringence in gases which depends on  $B^2$  exactly like vacuum magnetic birefringence. The magnetic birefringence of gases also depends linearly on pressure. In Table III the equivalent partial pressures  $P_{\text{eq}}$  which would mimic a vacuum magnetic birefringence for various gases [5, 26–28] are reported. The vacuum system must maintain these species well below their vacuum equivalent pressures. This is done by a combination of turbo molecular pumps (switched off during data taking) and non-evaporable getter pumps. The working pressure is below  $10^{-7}$  mbar, the main residual gas species being water.

Table III: Vacuum equivalent pressures  $P_{\text{eq}}$  for various gases.

Gas	$ \Delta n_u [\text{T}^{-2} \text{atm}^{-1}] $	$P_{\text{eq}} [\text{mbar}]$
He	$2.1 \times 10^{-16}$	$2 \times 10^{-5}$
Ar	$7 \times 10^{-15}$	$6 \times 10^{-7}$
H <sub>2</sub> O	$6.7 \times 10^{-15}$	$6 \times 10^{-7}$
CH <sub>4</sub>	$1.6 \times 10^{-14}$	$3 \times 10^{-7}$
O <sub>2</sub>	$-2.5 \times 10^{-12}$	$2 \times 10^{-9}$
N <sub>2</sub>	$-2.5 \times 10^{-13}$	$2 \times 10^{-8}$

### III. CALIBRATION

Calibration of the apparatus is done using the Cotton-Mouton effect. In this case we used low pressure oxygen, which gives large signals. More importantly, we have also checked the calibration of the apparatus with low pressure helium, so as to induce a small ellipticity and demonstrate the sensitivity of the entire system. The lowest pressure of helium used was  $P^{(\text{He})} = 32 \mu\text{bar}$ . Considering that the unitary birefringence ( $B = 1$  T and pressure = 1 atm) of helium due to the Cotton-Mouton effect is  $\Delta n_u^{(\text{He})} = (2.1 \pm 0.1) \times 10^{-16} \text{T}^{-2} \text{atm}^{-1}$  [26, 27], the birefringence induced @  $B = 2.5$  T and  $P = 32 \mu\text{bar}$  is  $\Delta n^{(\text{He})} = 3.9 \times 10^{-20}$ . In figure 2 the Fourier transform of the measured ellipticity signal  $\psi(t)$  is shown. There is a clear peak at  $2\Omega_{\text{Mag}}$ , corresponding to an ellipticity of  $(1.13 \pm 0.13) \times 10^{-7}$ , with no spurious peaks present at other harmonics. Given the values of  $\mathcal{F}$ ,  $\lambda$ , and  $\int B^2 dl$ , from the amplitude of the He peak at  $32 \mu\text{bar}$ , the value of  $\Delta n_u$  for helium results to be  $\Delta n_u^{(\text{He,PVLAS})} = (2.2 \pm 0.1) \times 10^{-16} \text{T}^{-2} \text{atm}^{-1}$ , in excellent agreement with other published values [5, 26, 27]. It must be noted that this value is obtained from a single low pressure point. Other two low pressure points were also taken. Figure 3 shows a graph of  $\Delta n^{(\text{He})}/B^2$  as a function of pressure  $P$ .

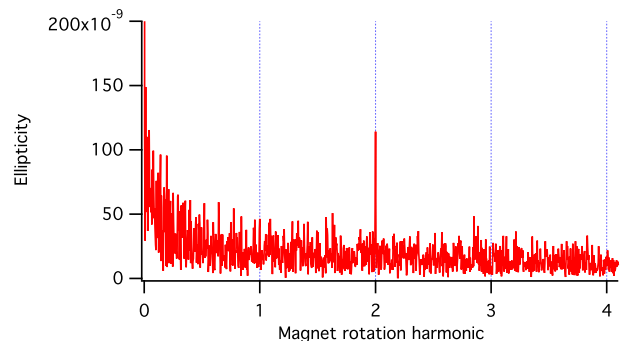


Figure 2: Fourier spectrum of the measured ellipticity  $\psi(t)$  with  $32 \mu\text{bar}$  pressure of He. The integration time was  $T = 4$  hours. The peak at  $2\Omega_{\text{Mag}}$  corresponds to  $\psi = 1.13 \times 10^{-7}$ . The vacuum magnetic birefringence predicted by QED is equivalent to a He pressure of  $\sim 20$  nbar.

The calibration process also allows the determination of the physical phase of the Fourier components: the el-

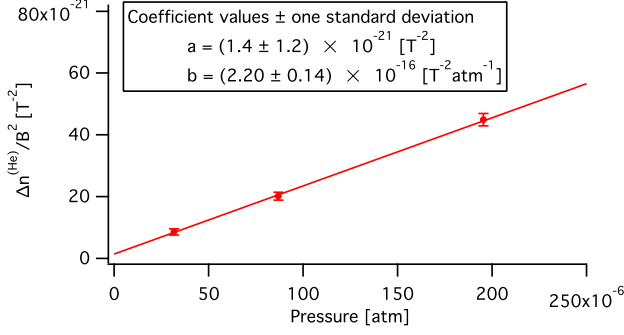


Figure 3: Measured  $\Delta n^{(\text{He})}/B^2$  as a function of pressure  $P$ . The error bars correspond to a  $1\sigma$  statistical error. The data are fitted with a linear function  $a + bP$ .

lipticity induced by a magnetic birefringence is maximum when the magnetic field is at  $\vartheta = \pm 45^\circ$  with respect to the polarisation direction. Since a magnetic birefringence can be either positive or negative, the physical phase is determined  $\text{mod } 180^\circ$ . A magnetically induced birefringence must have a phase consistent with the calibration phase. The ellipticity amplitudes determined from the Fourier transforms of the data obtained in vacuum are therefore projected along the physical and the non-physical axes.

#### IV. RESULTS

The data presented in this paper have been collected by rotating the two magnets at frequencies ranging from 2.4 Hz to 3 Hz for a total of 210 hours. Of these, 40 hours have been acquired with the magnets rotating at slightly different frequencies so as to check that neither of the two was generating spurious signals.

The data analysis procedure is as follows:

- 1) For each run, lasting typically one day, the acquired signals are subdivided in blocks of 8192 points (256 magnet revolutions) and a Fourier transform of the ellipticity signal  $\psi(t)$ , calculated using equation (7), is taken for each block.
- 2) For each block, the average noise in the ellipticity spectrum around  $2\Omega_{\text{Mag}}$  is taken. The ellipticity amplitude noise follows the Rayleigh distribution  $P(\rho) = (\rho/\sigma^2)e^{-\frac{\rho^2}{2\sigma^2}}$ , in which the parameter  $\sigma$  represents the standard deviation of two identical independent Gaussian distributions for two variables  $x$  and  $y$  and  $\rho = \sqrt{x^2 + y^2}$ . In our case  $x$  and  $y$  represent the projections of the ellipticity noise along the physical and the non-physical axes. The average of  $P(\rho)$  is related to  $\sigma$  by  $\langle P \rangle = \sigma\sqrt{\pi/2}$ . For each data block  $\sigma$  is determined. This value is used in the next step as the weight for the ellipticity value at  $2\Omega_{\text{Mag}}$ .
- 3) For each run, a weighted vector average of the Fourier

components of the ellipticities at  $2\Omega_{\text{Mag}}$ , determined in step 2), is taken.

- 4) Using the values for  $\mathcal{F}$ ,  $\int B^2 dl$ , and  $\lambda$  for each run,  $\Delta n/B^2$  and  $\sigma/B^2$  are determined. The value of  $\Delta n/B^2$  is then projected onto the physical and non-physical axes. These values are plotted in figure 4.

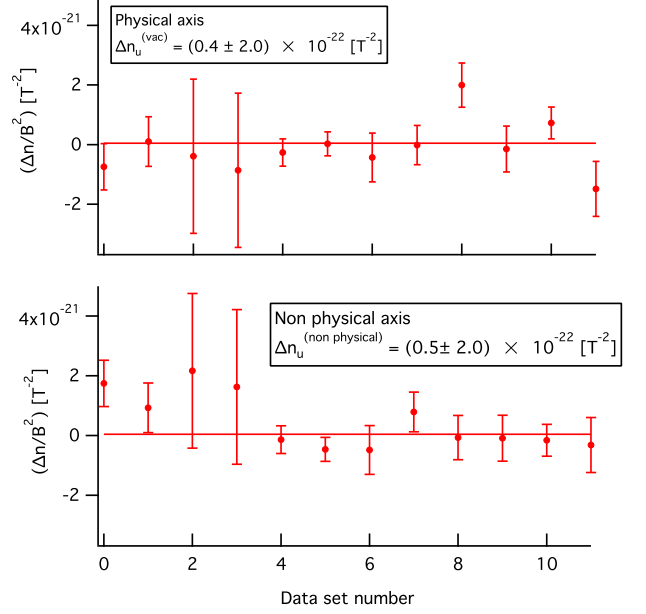


Figure 4: Projections of  $\Delta n/B^2$  along the physical and the non-physical axes for all the data sets. The horizontal red line represents the weighed average for all the runs.

The weighted vector average of all the runs results in a value for the unitary birefringence of vacuum, with a  $1\sigma$  error, of

$$\Delta n_u^{(\text{vac})} \pm \sigma_{\Delta n_u^{(\text{vac})}} = (4 \pm 20) \times 10^{-23} \text{ T}^{-2} \quad (8)$$

for the physical component (same phase and sign as for the helium Cotton-Mouton birefringence). For the non-physical component one finds  $\Delta n_u^{(\text{non physical})} \pm \sigma_{\Delta n_u^{(\text{vac})}} = (5 \pm 20) \times 10^{-23} \text{ T}^{-2}$ . These values are compatible with zero at a  $1\sigma$  level. Remembering that  $A_e = \Delta n_u^{(\text{vac})}/3$  and by using therefore  $\sigma_{\Delta n_u^{(\text{vac})}}/3$  as an upper limit on  $A_e$  one obtains

$$A_e < \frac{\sigma_{\Delta n_u^{(\text{vac})}}}{3} = 65 \times 10^{-24} \text{ T}^{-2}. \quad (9)$$

This new limit is about a factor 50 from the predicted QED value of equation (3),  $A_e = 1.32 \times 10^{-24} \text{ T}^{-2}$ , and a factor of about 20 better with respect to the previously published limits.

## V. DISCUSSION AND CONCLUSIONS

### A. QED

We have reported here on a significant improvement on the limit of non linear electrodynamic effects in vacuum. In the Euler-Heisenberg framework we are now only a factor 50 away from the theoretical parameter,  $A_e = 1.32 \times 10^{-24} \text{ T}^{-2}$ , describing these effects. This measurement represents the best limit on vacuum magnetic birefringence obtained so far. Our new limit is

$$A_e < 65 \times 10^{-24} \text{ T}^{-2} @ 68\% \text{ c.l.} \quad (10)$$

In figure 5 we compare previously published results with our new value and with the predicted QED effect.

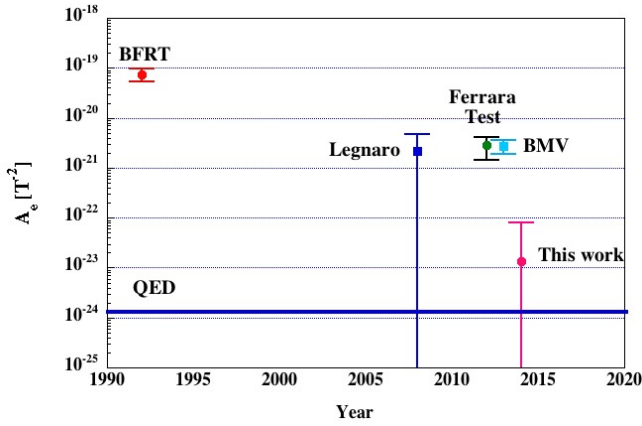


Figure 5: Comparison of published results for  $A_e$  of ellipsometric experiments (BFRT = [6], Legnaro = [13], Ferrara Test = [14], BMV = [23]). The error bars correspond to a  $1\sigma$  c.l.

Always in the Euler-Heisenberg framework, the elastic photon-photon total cross section for non polarized light also depends directly on  $A_e$ . In the limit of low energy photons,  $E_\gamma \ll m_e c^2$  [29–31],

$$\sigma_{\gamma\gamma}(E_\gamma) = \frac{973\mu_0^2}{20\pi} \frac{E_\gamma^6}{\hbar^4 c^4} A_e^2. \quad (11)$$

From the experimental bound on  $A_e$  one can therefore also place an upper bound on  $\sigma_{\gamma\gamma}$ :

$$\sigma_{\gamma\gamma} < 4.6 \times 10^{-66} \text{ m}^2 = 4.6 \times 10^{-23} \text{ fb} @ 1064 \text{ nm} \quad (12)$$

Although the sensitivity of our apparatus is far from its theoretical shot noise limit, integration in the absence of spurious peaks at the frequency of interest has allowed this significant improvement. Such a long integration time has been possible thanks to the choice of using high field permanent dipole magnets which do not need any kind of power supply or cooling. At present the ellipsometric technique is the most sensitive one for approaching low-energy non-linear QED effects. Efforts will now go into the improvement of the sensitivity.

### B. Axion like particles

To set new model independent limits on the coupling constant of axion-like particles (ALP) to two photons, only the runs with both magnets rotating at the same frequency were used, so that the total field length could be taken as the sum of the two magnet lengths.

The magnetic birefringence induced by low mass axion-like particles can be expressed as [6]

$$\Delta n^{(\text{vac:ALP})} = \frac{g_a^2 B^2}{2m_{a,s}^2} \left( 1 - \frac{\sin 2x}{2x} \right) \quad (13)$$

where  $g_a$  is the ALP - 2 photon coupling constant,  $m_a$  its mass,  $x = \frac{Lm_a^2}{4\omega}$ ,  $\omega$  is the photon energy and  $L$  is the magnetic field length. The above expression is in natural Heavyside-Lorentz units whereby  $1 \text{ T} = \sqrt{\frac{\hbar^3 c^3}{e^4 \mu_0}} = 195 \text{ eV}^2$  and  $1 \text{ m} = \frac{e}{\hbar c} = 5.06 \times 10^6 \text{ eV}^{-1}$ .

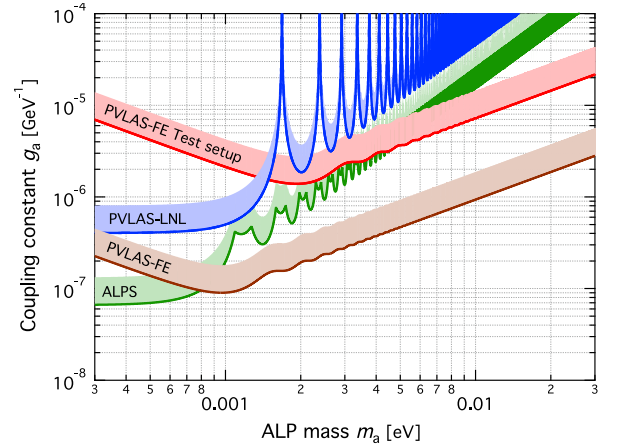


Figure 6: Updated exclusion plot for axion-like particles obtained from model-independent experiments. In green, limits from the ALPS collaboration [32]; in blue, limits from dichroism measurements performed by PVLAS at LNL [7]; in red, limits from the ellipticity measurements performed with the test setup in Ferrara [14]. The results described in this paper lead to a new bound, shown in brown.

In the approximation for which  $x \ll 1$  (small masses) this expression becomes

$$\Delta n^{(\text{vac:ALP})} = \frac{g_a^2 B^2 m_a^2 L^2}{48\omega^2} \quad (14)$$

whereas for  $x \gg 1$

$$\Delta n^{(\text{vac:ALP})} = \frac{g_a^2 B^2}{2m_a^2}. \quad (15)$$

From our limit on  $\Delta n_u^{(\text{vac})}$  given in equation (8) one can plot a new model independent exclusion plot for ALPs. Above  $10^{-3} \text{ eV}$  there is an almost 10 fold improvement on the upper limit of  $g_a$  with respect to previously published model independent limits.



### C. Millicharged particles

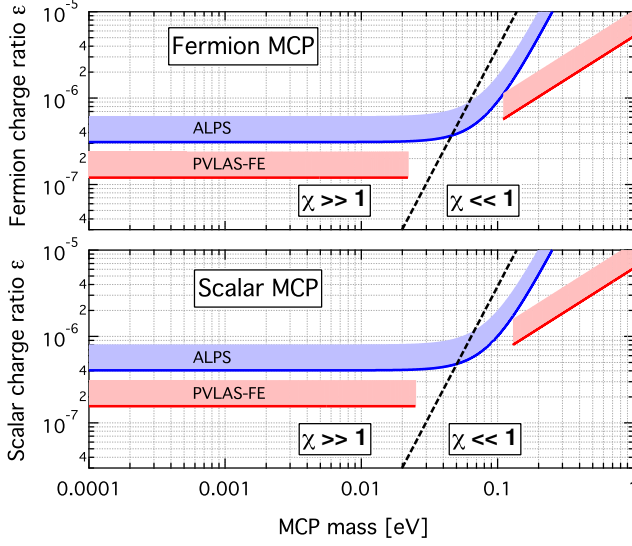


Figure 7: Updated exclusion plot for scalar and fermion millicharged particles. In blue is the previous limit taken from [36] and in red our new limits. The two branches of each of the red ellipticity curves are not connected in the mass range around  $\chi \simeq 1$  (dotted black line), where the difference of the indices of refraction changes sign.

Slightly better exclusion plots can also be derived from  $\Delta n_u^{(\text{vac})}$  for fermion and scalar millicharged particles. The vacuum magnetic birefringence due to the existence of such hypothetical millicharged particles can be calculated following [33–35]. By defining the ratio of the charge  $q$  of such particles to the charge of the electron  $\epsilon = q/e$  and  $\chi$  as

$$\chi \equiv \frac{3}{2} \frac{\hbar \omega}{m_\epsilon c^2} \frac{\epsilon e B \hbar}{m_\epsilon^2 c^2}. \quad (16)$$

it can be shown that

$$\Delta n^{(\text{vac:fermion})} = \begin{cases} 3A_\epsilon B^2 & (\chi \ll 1) \\ -\frac{9}{7} \frac{45}{2} \frac{\pi^{1/2} 2^{1/3} (\Gamma(\frac{2}{3}))^2}{\Gamma(\frac{1}{6})} \chi^{-4/3} A_\epsilon B^2 & (\chi \gg 1) \end{cases} \quad (17)$$

and

$$\Delta n^{(\text{vac:scalar})} = \begin{cases} -\frac{6}{4} A_\epsilon B^2 & (\chi \ll 1) \\ \frac{9}{14} \frac{45}{2} \frac{\pi^{1/2} 2^{1/3} (\Gamma(\frac{2}{3}))^2}{\Gamma(\frac{1}{6})} \chi^{-4/3} A_\epsilon B^2 & (\chi \gg 1) \end{cases} \quad (18)$$

where, in analogy to QED,  $A_\epsilon$  is

$$A_\epsilon = \frac{2}{45\mu_0} \frac{\epsilon^4 \alpha^2 \lambda_\epsilon^3}{m_\epsilon c^2}. \quad (19)$$

In figure 7 we show our new limit on  $\epsilon$  as a function of particle mass compared to a previous limit obtained from magnetically induced dichroism measurements [36]. In the case of fermions this includes neutrinos, for which  $\epsilon \lesssim 10^{-7}$  for masses below 20 meV. For previous limits see [37].

### Acknowledgements

We greatly thank Luca Landi for his invaluable technical help during the construction of the apparatus.

- 
- [1] H. Euler and B. Kochel, *Naturwiss.* **23**, 246 (1935).  
W. Heisenberg and H. Euler, *Z. Phys.* **98**, 718 (1936).  
V.S. Weisskopf, *Kgl. Danske Vid. Sels., Math.-fys. Medd.* **14**, 6 (1936).  
J. Schwinger, *Phys. Rev.* **82**, 664 (1951).
  - [2] P. A. M. Dirac, *Proc. R. Soc. Lond. A* **117**, 610 (1928); **126**, 360 (1930).
  - [3] C. D. Anderson, *Phys. Rev.* **43**, 491 (1933).
  - [4] R. Baier and P. Breitenlohner, *Acta Phys. Austriaca* **25**, 212 (1967); *Nuovo Cimento* **47**, 261 (1967).  
S.L. Adler, *Ann. Phys.* **67** (1971) 559.  
Z. Bialynicka-Birula and I. Bialynicki-Birula, *Phys. Rev. D* **2**, 2341 (1970).
  - [5] C. Rizzo, A. Rizzo, and D. M. Bishop, *Int. Rev. Phys. Chem.* **16**, 81 (1997).
  - [6] R. Cameron *et al.*, *Phys. Rev. D* **47**, 3707 (1993).
  - [7] E. Zavattini *et al.*, *Phys. Rev. D* **77**, 032006 (2008).
  - [8] W.-T. Ni, *Chin. J. Phys.* **34**, 962 (1996).
  - [9] H.-H. Mei *et al.*, *Mod. Phys. Lett. A*, **25**, 983 (2010).
  - [10] P. Pugnati *et al.*, *Czech. J. Phys. A* **56**, C193 (2006).
  - [11] E. Iacopini and E. Zavattini, *Phys. Lett.* **85B**, 151 (1979).
  - [12] D. Bakalov *et al.*, *Hyperfine Interact.* **114**, 103 (1998).
  - [13] M. Bregant *et al.*, *Phys. Rev. D* **78**, 032006 (2008).
  - [14] F. Della Valle *et al.*, *New J. Phys.* **15**, 053026 (2013).
  - [15] F. Della Valle *et al.*, *Nucl. Instrum. Methods Phys. Res. A* **718**, 495 (2013).
  - [16] R. Battesti *et al.*, *Eur. Phys. J. D* **46**, 323 (2008).
  - [17] D. Bernard *et al.*, *Eur. Phys. J. D* **10**, 141 (2000).
  - [18] F. Moulin, D. Bernard, and F. Amiranoff, *Z. Phys. C* **72**, 607 (1996).
  - [19] E. Lundström *et al.*, *Phys. Rev. Lett.* **96**, 083602 (2006).
  - [20] D. Tommasini *et al.*, *Phys. Rev. A* **77**, 042101 (2008).
  - [21] A.N. Luiten and J. C. Petersen, *Phys. Rev. A* **70**, 033801 (2004); *Phys. Lett. A* **330**, 429 (2004).

- [22] E. Milotti *et al.*, Int. J. Quantum Inform. **10**, 1241002 (2012).
- [23] A. Cadène *et al.*, Eur. Phys. J. D **68**, 16 (2014).
- [24] F. Della Valle *et al.*, Opt. Expr. **22**, 11570 (2014).
- [25] G. Cantatore *et al.*, Rev. Sci. Instrum. **66**, 2785 (1995).
- [26] M. Bregant *et al.*, Chem. Phys. Lett. **471**, 322 (2009) .
- [27] A. Cadène *et al.*, Phys. Rev. A **88**, 043815 (2013).
- [28] F. Della Valle *et al.*, Chem. Phys. Lett. **592**, 288 (2014).
- [29] B. De Tollis, Nuovo Cimento **35**, 1182 (1965); **32**, 757 (1964).
- [30] R. Karplus and M. Neuman, Phys. Rev. **83**, 776 (1951).
- [31] D. A. Dicus, C. Kao, and W. W. Repko, Phys. Rev. D **57**, 2443 (1998).
- [32] K. Ehret *et al.* Phys. Lett. B **689**, 149 (2010).
- [33] W.-y. Tsai and T. Erber, Phys. Rev. D **12**, 1132 (1975).
- [34] J. K. Daugherty and A. K. Harding, Astrophys. J. **273**, 761 (1983).
- [35] M. Ahlers, *et al.*, Phys. Rev. D **75**, 035011 (2007).
- [36] M. Ahlers, *et al.*, Phys. Rev. D **77**, 095001 (2008).
- [37] K. Nakamura *et al.* (Particle Data Group), J. Phys. G **37**, 075021 (2010), p. 557.